

Designing Rear View Mirror of Car Using CFD and Reverse Engineering

Balendra V.S.Chauhan^{*,****}, Ajitanshu Vedrtam^{*,**,***}
and Virendra Pratap^{****}

Keywords : CFD; Drag Reduction; Rear view mirror; Passenger car; Reverse engineering.

ABSTRACT

The rear-view mirror (RVM) of a Maruti Suzuki RITZ car was modeled using the reverse engineering (RE) and further the design of RVM is modified using CATIA. A Computational fluid dynamics (CFD) model was built to investigate the wake structure and the vortex body frame interaction near the unmodified and modified RVM of a car. The velocity vector fields in the wake and pressure distribution over the RVM skin were measured at Reynolds number of 2.6×10^5 using ANSYS fluent software. The results of CFD model for unmodified and modified RVM designs are compared and consequently, the accuracy of the CFD analysis is validated from the manual calculation. The validation of CFD model was ensured by the experimentation using an open circuit blow down type wind tunnel. Once, the CFD model was validated, the design alterations are applied to the geometry of RVM with an aim of drag reduction. The CFD analysis of feasible RVM design modification reported a maximum of 45.7% drag reduction at a velocity of 108 km/h.

INTRODUCTION

Fuel economy and the lesser emissions can be achieved by improving propulsion system or by reducing the aerodynamic drag. The drag reduction in the vehicles became more significant at the higher speed (more than 60 km/h. Drag reduction of the cars is widely discussed in the literature (Koike et. al., 2004; Singh et. al., 2005; Desai et. al., 2005; Rouméas et. al., 2009; Joseph 199). Among the many parts of the car contributing to drag, RVM has 2-7 % contribution in drag increment (Hucho and Sovran, 1993).

Paper Received June, 2018. Revised July, 2019. Accepted August, 2019. Author for Correspondence: Ajitanshu Vedrtam

^{*}Department of Mechanical Engineering, Invertis University, Bareilly, UP, India-243001

^{**}Vinoba Bhawe Research Institute, Allahabad, UP, India-211004.

^{***}Translational Research Centre, Institute of Advanced Materials, VBRI, Linköping 58330, Sweden

^{****}Department of Mechanical Engineering, Galgotia University, UP, India-201307

ajitanshu.m@invertis.org*

within a plastic housing for an indirect vision that facilitates observance the traffic area adjacent and behind the car (Vachss, et. al. 1996; Pollard 1993). The efforts to modify the design of RVM for drag reduction are constrained by the legal safety standards (The European Parliament and The Council of the European Union Directive, 2003). Still, the small changes in edges radius, adding gutters, changing inclinations, edges, and housing curvature may reduce the drag. The material modification is also attempted in the literature for the drag reduction (Lim, et. al. 2017) along with the passive and active flow control methods (Cattafesta and Sheplak, 2011; Brunton and Noack, 2015; Vernet, 2015). An additional constraint to be considered while designing RVM is the reduction of the mirror fluctuations due to the acoustic noise. As the complex three-dimensional housing geometries are difficult to model, reverse engineering (RE) methods could be a good possible option to draw the geometries of the housings (Gao et. al. 2009).

The wake pattern generated by the mirror housing depends on the flow induced by the car front (the bonnet, fender, and windshield). The wake structure around RVM is discussed widely in the cited literature (Kim et. al., 2008; Khalighi et. al. 2008; Oswald 1999; Watkins and Oswald 1999; Jaitlee et. al. 2007; Lounsberry, 2007; Dolek et. al., 2004; Ono et. al., 1999; Chen et. al., 2009; Rind and Hu, 2007). Due to the RVM, a vortex wrap is formed that moves along the car body skin and generates an interaction noise (Kim et. al., 2008). The wake structure depends on the geometry of RVM, however, mostly the velocity profiles in the inner near-wake of individual RVM has the large momentum shortfall and locally the main flow accelerates near the edge of the RVM (Khalighi et. al., 2008). The vibrations in the RVM are caused by the mechanical (rotational imbalance of the engine, road surface condition) and aerodynamic sources (Karman-type periodic wake, A-pillar vortex) collectively (Oswald, 1999). It was reported by Watkins and Oswald (1999) that even the small rotation about the horizontal or the vertical axis of the RVM surface causes vibrations. Jaitlee et al. (2007), have reported that the maximum fluctuating pressure (which was not uniformly distributed) acted at the central bottom region of RVM. An effort to reduce the

fluctuation pressure is made by extending the outer periphery of the RVM. Lounsberry et al. (2007), found that a whistle like sounds radiates from the mirror housing when the transition to a turbulent boundary layer over the RVM is not completed. The pressure fluctuations near the trailing edges of the RVM cause a rapid change in the flow patterns results in the whistle noise. Dolek et al. (2004), have also reported the generation of an intrinsic noise due to the mounted RVM. Ono et al. (1999) highlighted the wind noise radiated from the RVM and A-pillar through pressure fluctuations (measured using the Light-hill acoustic analogy). Chen et al. (2009) presented the wind noise characteristics generated by the RVM. It was reported that the pressure level that caused the highest noise was in the highly-separated flow region. Rind and Hu (2007) Investigated the aerodynamic performance of a Formula-1 car RVM (a simplified two-dimensional model at the different Reynolds numbers) varying the location of its glass inside the housing. A strong correlation between the mirror’s glass location and its drag over all investigated Reynolds numbers ranging from 1.1×10^5 to 2.6×10^5 was reported during the experimentation. It was found that as the mirror’s glass is located further inside the frame a 10%-11% drag is reduced. No change was observed in the mirror’s vortex shedding frequency at all the investigated Reynolds numbers, which implies that there was no structural impact of this modification. However, the computational results obtained using Fluent failed to predict the changes in flow characteristics and drag caused by the proposed modification. It was recommended that further calculations are needed using a higher order numerical methods to confirm the experimental findings. Woyczynski et. al. (2014) reported a passive jet flow control as applied to an automotive side-view mirror with some success.

Most of the cited articles were focused on the reduction of the noise emanating, the vibration of RVM, and experimental determination of RVM location. An improved CFD model devoted to reducing drag while following the legal requirement is still required. The objectives of the present work include obtaining an optimized design of RVM resulting the lesser drag via experimentally validated CFD model. CFD and RE both can complement each other very well, however, this combination is less frequently cited in the available literature. The use of RE for quickly and accurately obtaining the geometry of RVM is presented. The modifications made to the geometry of RVM were made considering the today’s regulations and legal demands.

MATERIALS AND METHODS

Figure 1 demonstrates the stepwise method adopted for the present study for obtaining model of RVM. To obtain the point cloud representing the geometry of RVM, COMET L3D scanner setup was

used. Firstly, the RVM was placed on the rotating table and a light is projected on RVM by a sensor unit. The projected light enabled the camera placed below the RVM to record several images in IGES, STEP, and STL formats. These images were used to obtain the point cloud (consisting around 2 million high-precision 3D coordinate points) representing the geometry of RVM. The point cloud was converted into usable images by the COLIN3D software.

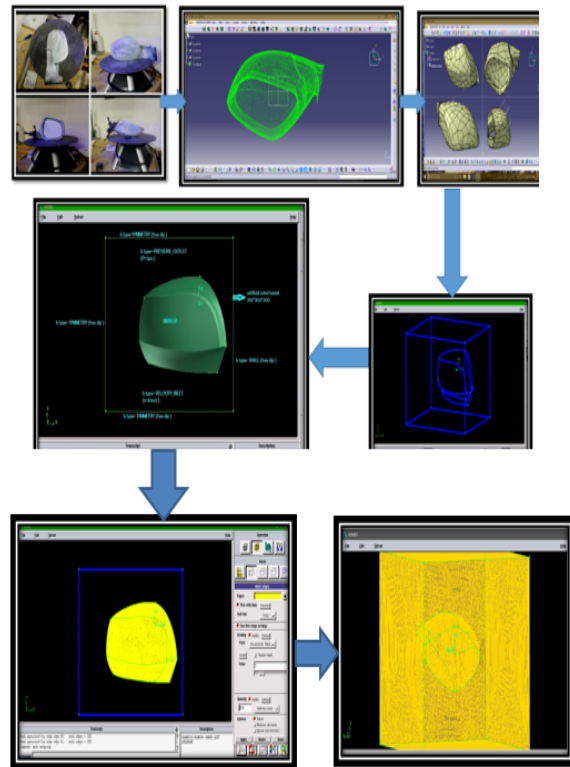


Fig 1 – Stepwise method used for modeling RVM

Further, for the creation of a 3D solid CAD file from the point cloud data, the data file is imported into the Digitized Shape Editor module of CAD software (CATIA V5). The CATIA V5 automatically detected and removed any redundant and undesirable points from the RVM profile for the smooth 3D-mesh generation. Further, the Quick Surface Reconstruction module was used to draw the curves over the mesh using 3D curve creation module. The data file representing the geometry of RVM is extracted in .IGES format from CATIA to import in GAMBIT 2.2.3 software for the meshing. The details of meshing are given in Tables 1-3.

Table 1. Dimension of outer domain.

X	350 mm
Y	300 mm
Z	300 mm

Table 2. Number of grid generate on the edges of the RVM.

Mesh edge	Number of grids taken
Edge 01	096
Edge 02	222
Edge 03	140
Edge 04	064
Edge 05	056
Edge 06	046
Edge 07	264
Edge 08	020
Edge 09	100
Edge 10	076
Edge 11	132
Edge 12	176
Edge 13	294
Edge 14	162

Table 3. Number of grid generate on the edges of the domain.

Mesh edge	Number of grid taken
Edge 15,19,23,26	350
Edge 16,17,24,25	300

Moreover, the boundary conditions were specified (Table 4) for the flow characteristics on the boundaries of the computational model. The unstructured meshing was considered for the RVM faces due to the complex structure. The parameters considered for face meshing are given in Table 5. The numbers of elements formed on faces are given in Table 6.

Table 4. Boundary condition of the domain.

Inlet	Velocity inlet
Outlet	Pressure outlet
Upper and lower domain	Symmetry
Right domain	Wall
Left domain	Symmetry
Mirror body	Wall

Table 5. Face meshing type.

Element	Quad
Type	Pave
Interval sizing / spacing	1

Table 6. Number of element formed on faces.

Face mesh	Number of elements generated
Face 1	09955
Face 2	11691
Face 3	06022
Face 4	29303
Face 5	21860
Face 6	08416
Face 7	15116

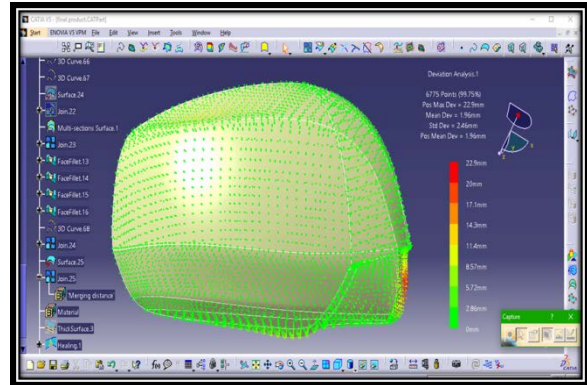


Fig. 2 Deviation between the unmodified and modified RVM.

The deviation between the originally scanned RVM and the modified RVM is shown in Figure. 2. The results of deviation check on 6775 points (approximately equal to 99.75% of the total surface covered by the points are given in Table 7.

Table 7. Results of deviation analysis.

Total number of points	6775
Pos max deviation	22.9mm
Mean deviation	1.96mm
Standard deviation	2.46mm

For the validation of CFD model, the drag coefficient for the RVM of a Maruti Suzuki RITZ car was measured in open circuit blow down type wind tunnel at 30 m/s inlet velocity. The wind tunnel was consisting: driving unit (blower), High-Efficiency Particulate (HEPA) filter, wide angle diffuser, settling chamber, contraction cone, small entry duct (expander) and a rectangular test section. The delivery pressure of 0.6 m of the water column was provided by a single stage centrifugal blower ('SMW' make) having a capacity of 0.6 m³/s. An 11kW electric induction motor (Compton Greaves make) with a rated speed of 2920 rpm was coupled to the blower. Intake airflow from the blower exit was controlled using the throttling mechanism at the blower inlet. A flexible coupling was used to connect the blower outlet with the conical diffuser for the lesser vibrations. A HEPA filter was used at the suction side of the blower to trap the micro-particles (99.97% of 0.3 μm diameter) laden in the air. The discharge from the blower enters a conical diffuser of the 2-meter length, 0.22-meter, 0.6-meter inlet and outlet diameters respectively. The discharge from the diffuser enters the settling chamber having a 0.6-meter diameter and 1.5-meter length. Nylon screens were used at the three different locations within the settling chamber for the straightening and the turbulence level reduction of the flow before it enters the contraction cone. A contraction cone, shaped as bell-mouth and made of Fibre-reinforced plastic (FRP), having a length of

0.45m was fitted at the exit of the settling chamber. It helps in achieving uniform velocity profile at the exit of the contraction cone by reducing the turbulence fluctuation. An area contraction ratio (outlet to inlet area ratio) of 64:1 ensures a nearly uniform and low turbulence intensity flow at the test section entrance. A short transition type entry duct with the circular inlet of 0.075m and square outlet of 0.65 X 0.65m and length of 0.15 m was fitted at the end of the contraction cone. It helps to fix the diffuser of inlet size of 0.65 X 0.65m². The test section was made with transparent Perspex sheet. It has an outer dimension of 300 X 300 X 1500mm. The internal cross-section was reduced to 300 X 75mm with the help of pairs of parabolic wooden blocks 300 mm long X 75mm height and Perspex sheets. The gap of 300 X 75mm created at the top and bottom was used to keep the pressure tapping tubes untangled. To understand the flow field, a telescopic pitot tube, a calibrated five-hole probe with the transverse mechanism, a digital micro-manometer coupled with a pressure scanner and a digital metal vane anemometer were available with the wind tunnel [Vedrtnam and Sagar (2018, 2019)]. The RVM was placed on a rectangular platform connected through a threaded stud to a six-component force sensor made by JR3 Inc, USA, from which the value of Cd can be directly obtained. The variation of the drag coefficient with time was recorded on the attached personal computer as required for the validation of the CFD model.

RESULTS AND DISCUSSION

One of the objectives of the present study is to better understand the flow field around the RVM. The simulated artificial wind tunnel shows the fluid flow around the RVM and regions having flow separation. These flow separation regions are critical for drag generation. It is important to understand the locations of these separation regions because of the high amount of form drag that they create as well as wake generated. Table 8 shows the solution setup for the base model as well as the modified model.

Table 8. Solution setup for the base model as well as modified model.

Parameter	Value/Type
Type	Pressure based
Velocity formulation	Absolute
Time	Transient
Viscous	Laminar
Fluid	Air
Density	1.225kg/m ³
Viscosity	1e-05kg/m-s
Inlet velocity	30m/s
Pressure outlet	0 Pa
Ratio of specific heat	1.4
Transient formulation	Second order implicit

Initialization method	Standard method
Compute from	Inlet
Time step method	Fixed
Time step size for base model	0.616
Time step size for modified RVM	0.561
Number of time step	40000
Maximum iteration / time step	20

Figures 3 and 4 illustrate the velocity streamline flow and the air particles flow (instantaneous flow visualization) for the actual RVM geometry and modified RVM geometry respectively. Fig. 3 and Fig. 4 reflects that for the unmodified RVM the crude angle at the top and bottom edge of the RVM make the flow field vulnerable and boundary layer separates from the solid body much early. Therefore, a big separation bubble produces downstream of the RVM which delay the attachment of shear layer from both ends of the RVM. The big separation produces negative velocity (velocity opposite to the direction of main flow) and increases drag to a high extent. But for the modified RVM due to the smoothen surface and changed acute angle of the mirror, the boundary layer separation point from the body moves downstream over the surface of the mirror and produces small downstream separation. Therefore, a shear layer reattachment point moves upstream as compare to unmodified RVM and drag reduces to a large extent.

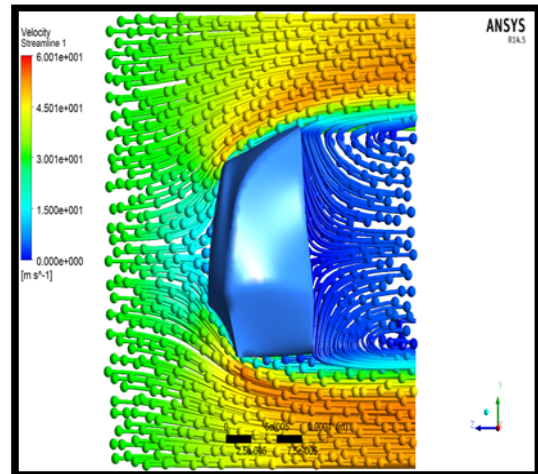
Figure 5 reflects that for unmodified RVM, some streamlines present at the upper and lower corner of the mirror are having haphazard direction indicating very rough boundary layer at the mirror's extreme ends. This is the major reason for the high separated zone in unmodified RVM, the boundary layer smoothen over the modified mirror surface which reducing the downstream separation zone.

Figures 6 and 7 demonstrate the fifteen levels of the pressure contour in which the unmodified RVM has the maximum pressure of 1988 Pa and up to 5th contour level a pressure level of 1167 Pa which is more than the maximum pressure observed (1077 Pa at same velocity inlet) by the modified RVM.

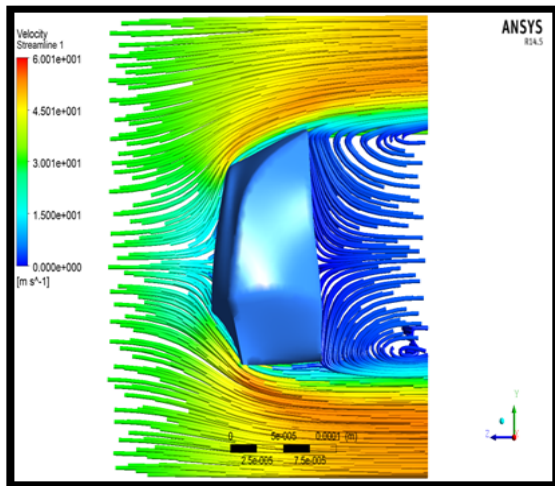
Figure 8 shows the pressure difference at front and back portion on the mirror. The leading surfaces of the RVM mirror there are high levels of static pressure. This occurs due to the presence of front stagnation point of the mirror upstream surface, because at front stagnation point the whole kinetic energy is converted into pressure energy. It can also be observed that on the trailing faces the static pressure is comparatively low, and thus this pressure difference is a major contributor to the RVM pressure drag and therefore its overall drag. Due to the high-pressure difference between front and back side of RVM a big separation bubble produced downstream of the RVM is also responsible for this high drag. As the mirror is

modified, the edges of the RVM is more curvatures which increased the aerodynamics of RVM and the downstream low-pressure zone reduces, which ultimately reduces the overall drag.

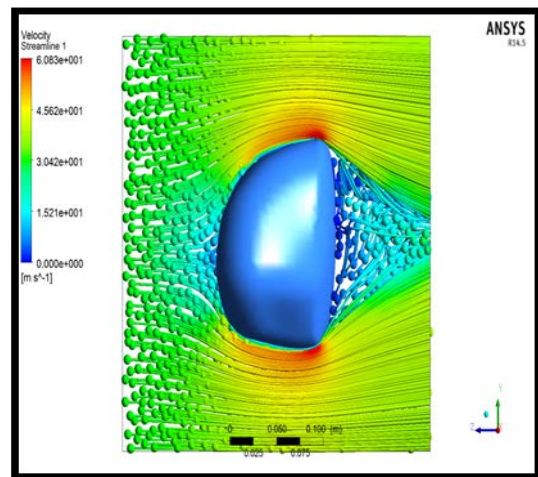
The variation of coefficient of drag (CD) with respect to the flow time is shown in figures9 and 10 for the basic model of RVM and the modified RVM model respectively. The fluctuations in CD graph for both the cases establish the flow field for the RVM was always remained turbulent. But interestingly as it can be observed that the distribution of CD value (rms of CD, CDrms) is much higher in case of unmodified RVM, which signifies a disturbed downstream flow field with bigger separation bubble behind the RVM. The modified RVM case represents a much smoother CD distribution, which signifies much smaller CDrms and therefore the downstream vortex becomes smaller.



(a)

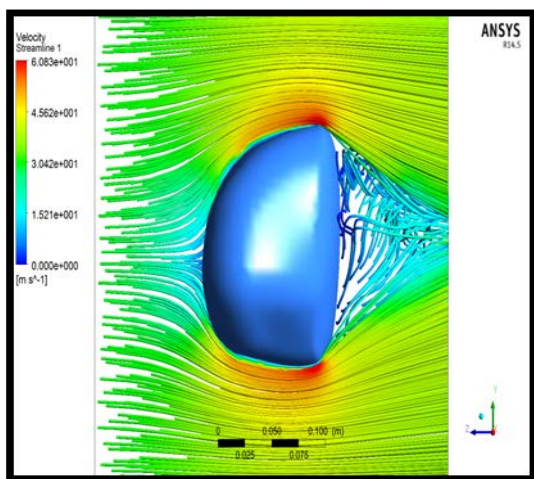


(a)



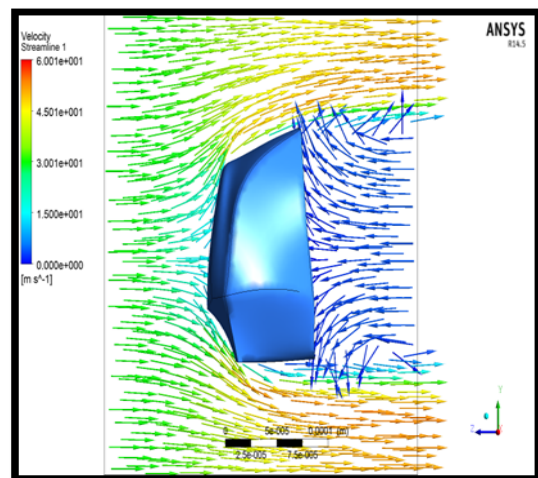
(b)

Figure 4. (a) & (b) Velocity streamline flow of air particles.

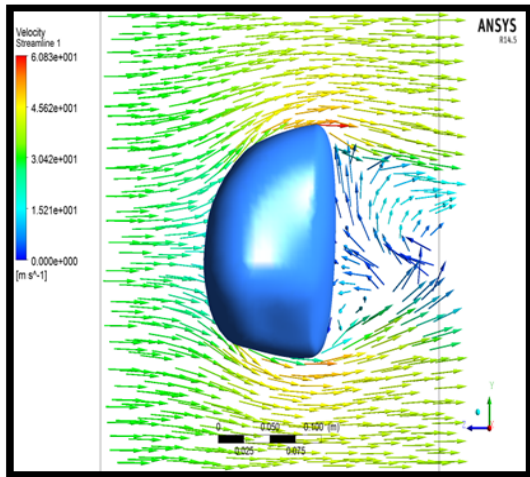


(b)

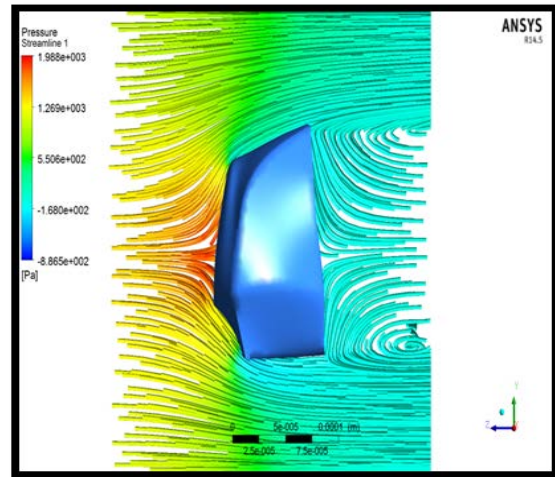
Figure 3. (a) & (b) Velocity streamline flow through the base model and modified RVM



(a)



(b)



(a)

Figure 5. (a) & (b) Flow direction of velocity streamline.

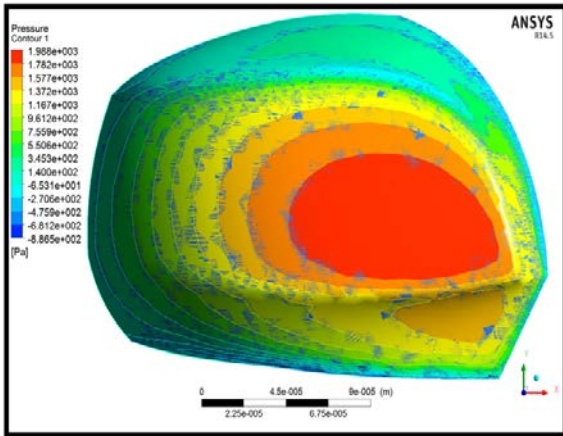
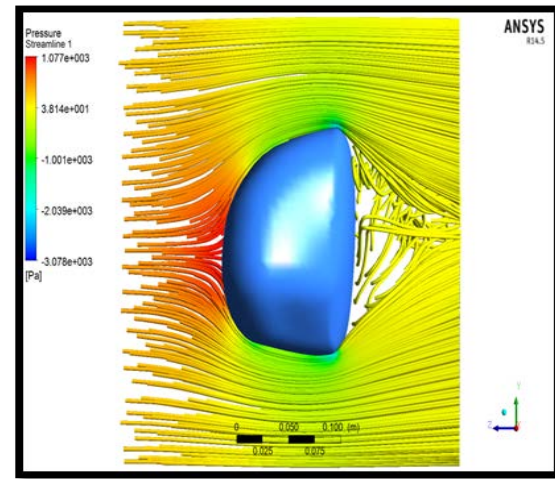


Figure6. Pressure contour of Unmodified RVM



(b)

Figure8. (a) & (b) Pressure difference at front and back portion on the mirror

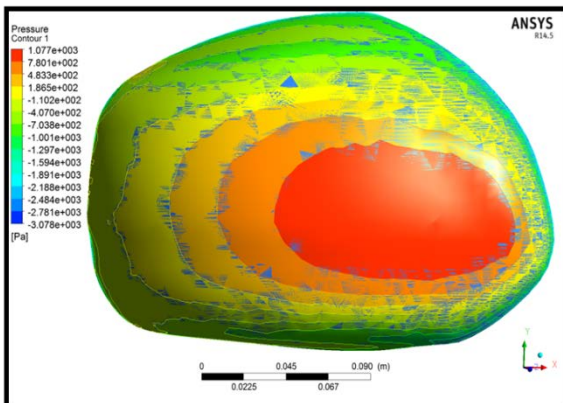


Figure7. Pressure contour of modified RVM.

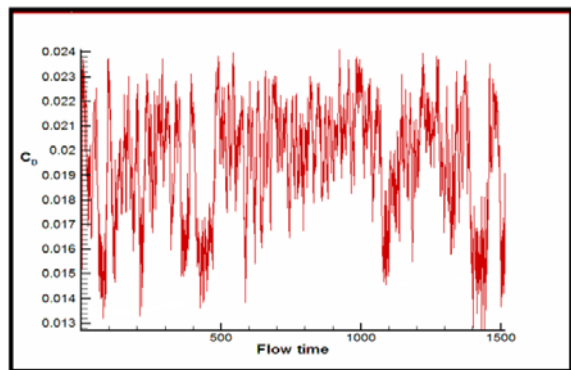


Figure 9. C_D vs. Flow time graph of base model of RVM

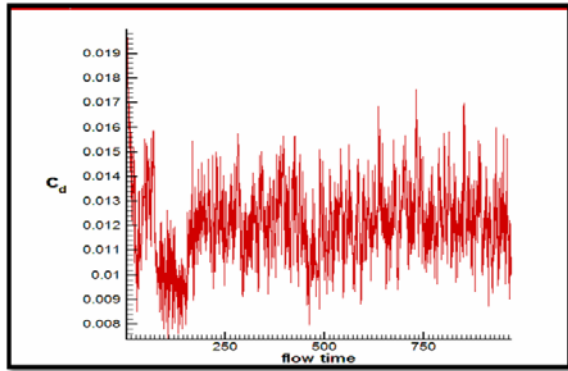


Figure 10. CD vs Flow time graph of modified RVM.

Table 9 shows that the modified RVM has 36 % lesser drag and 45.7% reduction in drag force at a speed of 108 km/h.

Table 9. Drag Comparison

Configuration	Original RVM	Modified RVM
C_D	0.019	0.012
% of C_D reduce from the original RVM	0	36%
F_D	2.01096 N	1.04186 N
% of F_D reduce from the original RVM	0	45.7%

The validation of the CFD model was performed for unmodified RVM used in modeling. The variation of C_D for the simulation results was from 0.0119 to 0.0241 with a mean of 0.019. For the experiment, the value of C_D varied from 0.01 to 0.24 with a mean of 0.0176, which is an excellent match. Fig. 11 shows the plot between C_D and flow time obtained from the experimentation.

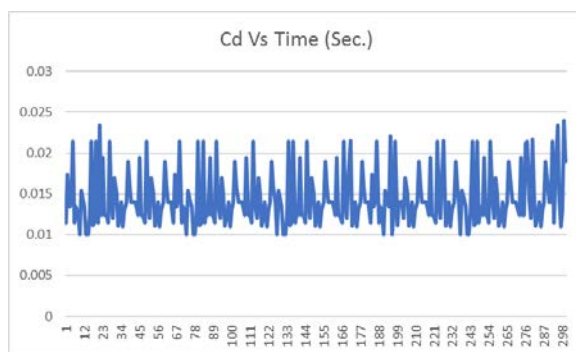


Figure 11. CD vs. Flow time graph of base model of RVM (Experiment)

CONCLUSIONS

The use of 3D scanning in RE processes for collecting the design data may contribute significantly to modeling. The flow separation regions were identified, which were mostly the sharp edges of the

RVM housing. The sharp edges and surface were modified by providing the taper at the edges and smoothening of the surface. In the modified RVM due to smoothen surface and modified acute angle of the mirror, the boundary layer separation point was delayed and small downstream separation was found. The modifications also significantly reduced the pressure drop at RVM surface. This optimization effort towards reducing the RVM drag was proved successful with a resulting reduction in drag of 45.7% from a speed of 108 km/h. The CFD model was validated as the results of simulation and experimentation were close enough. A parametric variation (keeping legal constraint intact) and flow control means could be applied for further optimizing the design of RVM. The detailed study on RVM surface vibration, intrinsic noise, turbulent characteristics, and spectral measurements could also reveal interesting results useful for designing RVM. The aerodynamics of the RVM is considered completely detached from the aerodynamics of the rest of the car. A future work may include modification of RVM with the connected portion of car to RVM, to observe the actual reduction in drag in the vehicle.

ACKNOWLEDGMENT

Present work is supported by IAAM, Sweden and Invertis University, Bareilly, (U.P.), India.

REFERENCES

- Brunton, S.L., Noack, B.R., 2015. Closed-loop turbulence control: progress and challenges. University of Washington Seattle, Seattle, Washington, Appl. Mech. Rev. 67. DOI: 10.1115/1.4031175.
- Chen, K., Johnson, J., Dietschi, U., and Khalighi, B., "Wind Noise Measurements for Automotive Mirrors," SAE Int. J. Passeng. Cars – Mech. Syst. 2(1): 419-433, 2009, DOI: <https://doi.org/10.4271/2009-01-0184>.
- Cattafesta III, L.N. and Sheplak, M., 2011. Actuators for active flow control. Annual Review of Fluid Mechanics, 43, pp.247-272.
- Desai, M., Channiwala, S.A. and Nagarsheth, H.J., 2008. Experimental and computational aerodynamic investigations of a car. WSEAS Transactions on Fluid Mechanics, 4(3), pp.359-366.
- Dölek, Ö., Özkan, G. and Özdemir, I.B., 2004. Structures of flow around a full scale side mirror of a car with relevance to aerodynamic noise. Proceedings of the Institution of Mechanical Engineers, Part D: Journal of Automobile Engineering, 218(10), pp.1085-1097.

- Gao, J., Chen, X., Zheng, D., Yilmaz, O. and Gindy, N., 2006. Adaptive restoration of complex geometry parts through reverse engineering application. *Advances in Engineering Software*, 37(9), pp.592-600.
- Hucho, W. and Sovran, G., 1993. Aerodynamics of road vehicles. *Annual review of fluid mechanics*, 25(1), pp.485-537.
- Joseph, K., 1995. *Race Car Aerodynamics Designing For Speed. Ch-2: Aerodynamic Forces and Terms (Page No: 40-44) &, pp.179-185.*
- Jaitlee, R., Alam, F. and Watkins, S., 2007. Pressure fluctuations on automotive rear view mirrors (No. 2007-01-0899). SAE Technical Paper.
- Koike, M., Nagayoshi, T. and Hamamoto, N., 2004. Research on aerodynamic drag reduction by vortex generators. *Mitsubishi motors technical review*, 16, pp.11-16.
- Kim, J.H., Han, Y.O., Lee, M.H., Hwang, I.H. and Jung, U.H., 2008. Surface flow and wake structure of a rear view mirror of the passenger car. *Proceedings of the Bluff Bodies Aerodynamics & Applications (BBAA) VI, Milan, Italy*, pp.20-24.
- Khalighi, B., Chen, K.H., Johnson, J.P., Snegirev, A., Shinder, J. and Lupuleac, S., 2013. Computational and experimental investigation of the unsteady flow structures around automotive outside rear-view mirrors. *International Journal of Automotive Technology*, 14(1), pp.143-150.
- Lounsberry, T.H., Gleason, M.E. and Puskarz, M.M., 2007. Laminar flow whistle on a vehicle side mirror. *SAE Transactions*, pp.1475-1480.
- Lim, G.H., Choi, H.J., Renou, F. and Roy, A.N., 2017. Effects of hydrophobic modification of xanthan gum on its turbulent drag reduction characteristics. *Journal of industrial and engineering chemistry*, 54, pp.146-150.
- Oswald, G., 1999. *Influence of Aerodynamics on the Operating Performance of Automotive External Rear View Mirrors (Doctoral dissertation, Royal Melbourne Institute of Technology).*
- Ono, K., Himeno, R. and Fukushima, T., 1999. Prediction of wind noise radiated from passenger cars and its evaluation based on auralization. *Journal of Wind Engineering and Industrial Aerodynamics*, 81(1-3), pp.403-419.
- Pollard, C.A., Sony Corp, 1993. Rear vision system for two-wheeled vehicles with movable handlebars. U.S. Patent 5, 243, 417.
- Rouméas, M., Gilliéron, P. and Kourta, A., 2009. Drag reduction by flow separation control on a car after body. *International journal for numerical methods in fluids*, 60(11), pp.1222-1240.
- Rind, E. and Hu, Z.W., 2007. Aerodynamics of F1 car side mirror.
- Singh, S.N., Rai, L., Puri, P. and Bhatnagar, A., 2005. Effect of moving surface on the aerodynamic drag of road vehicles. *Proceedings of the Institution of Mechanical Engineers, Part D: Journal of Automobile Engineering*, 219(2), pp.127-134.
- The European Parliament and The Council of the European Union Directive 2003/97/EC, Europe (2003)
DOI: <http://data.europa.eu/eli/dir/2003/97/oj>.
- Vachss, F.R., Southwell, W.H., Malus, J. and Khoshnevisan, M., Boeing Co, 1996. Automotive rear view mirror system. U.S. Patent 5,559,640.
- Vernet, J.A., Örlü, R. and Alfredsson, P.H., 2015. Separation control by means of plasma actuation on a half cylinder approached by a turbulent boundary layer. *Journal of Wind Engineering and Industrial Aerodynamics*, 145, pp.318-326.
- Vedrtnam, A. and Sagar, D., 2019. Experimental and simulation studies on aerodynamic drag reduction over a passenger car. *International Journal of Fluid Mechanics Research*, 46(1).
- Vedrtnam, A. and Sagar, D., 2018. Variation of drag coefficient, wall static pressure and secondary flow over passenger car. *International Journal of Automotive and Mechanical Engineering*, 15, pp.5002-5021.
- Watkins, S. and Oswald, G., 1999. The flow field of automobile add-ons—with particular reference to the vibration of external mirrors. *Journal of Wind Engineering and Industrial Aerodynamics*, 83(1-3), pp.541-554.
- Woyczynski, G., 2014. *Low Drag Automotive Mirror Using Passive Flow Jet Control*, Doctoral dissertation, University of Miami.